Optical properties and electronic band structure of $ZnIn_2Te_4$

Shunji Ozaki and Sadao Adachi
Department of Electronic Engineering, Faculty of Engineering, Gunma University, Kiryu-shi, Gunma 376-8515, Japan
(Received 6 November 2000; revised manuscript received 15 March 2001; published 8 August 2001)

Optical properties of the defect-chalcopyrite-type semiconductor $ZnIn_2Te_4$ have been studied by optical absorption, spectroscopic ellipsometry, and x-ray photoelectron spectroscopy. Optical absorption measurements suggest that $ZnIn_2Te_4$ is a direct-gap semiconductor having a band gap of ~1.40 eV. The complex dielectric-function spectra $\varepsilon(E)=\varepsilon_1(E)+i\varepsilon_2(E)$, measured by spectroscopic ellipsometry, reveal distinct structures at energies of the critical points in the Brillouin zone. Analysis of the numerically derived $\varepsilon(E)$ spectra facilitates the precise determination of the critical point parameters (energy position, strength, and broadening). By performing the band-structure calculation, these critical points are successfully assigned to specific points in the Brillouin zone. The measured x-ray photoelectron spectrum is also presented along with the density-of-states $N(E)$ calculation.

DOI: 10.1103/PhysRevB.64.085208 PACS number(s): 71.15.Dx, 78.20.Ci, 79.60.Bm

I. INTRODUCTION

The ternary semiconducting compounds $A^{II}B_2^{III}C_4^{VI}$ have been widely investigated because of their potential applications to electro-optic, optoelectronic, and nonlinear optical devices.[1] Most of these compounds have defect chalcopyrite (space group$=S_4^2$) or defect stannite (space group$=D_{2d}^{11}$) structure.[2] In an $A^{II}B_2^{III}C_4^{VI}$ defect chalcopyrite compound, *A*, *B*, and *C* atoms and the vacancy are distributed as follows.[3] *A* on $(a/2,0,c/4)$, *B* on $(0,0,c/2)$ and $(0,a/2,c/4)$, *C* on $(\alpha,\overline{\beta},\gamma)$, $(\overline{\alpha},\beta,\gamma)$, $(\beta,\alpha,\overline{\gamma})$, and $(\overline{\beta},\overline{\alpha},\overline{\gamma})$, and the vacancy on (0, 0, 0). $ZnIn_2Te_4$ is one of the defect chalcopyrite family and is known to have an ideal chalcopyrite structure;[2] i.e., its lattice parameters are simply given by $\alpha=\beta=a/4$, $\gamma=c/8$, and $c=2a$, as shown in Fig. 1. Although the material has been the subject of many research efforts, many fundamental properties have not been sufficiently evaluated or are even unknown.[3]

Very little is known about the optical properties of $ZnIn_2Te_4$. [4–9] Neumann *et al.*[4] studied the infrared reflectivity of $ZnIn_2Te_4$ in the wave number range from 170 to 4000 cm^{-1} at room temperature. The measured infrared reflectivity spectra were well described by a single harmonic oscillator model with transverse optical (TO) and longitudinal optical (LO) mode frequencies $\omega_{TO}=176\pm3\ cm^{-1}$ and $\omega_{LO}=198\pm4\ cm^{-1}$, respectively. They also determined the mean optical (high-frequency) dielectric constant $\varepsilon_\infty=(1/3)(2\varepsilon_{\infty\perp}+\varepsilon_{\infty\parallel})$ to be 7.1 ± 0.3,[5] where $\varepsilon_{\infty\perp}$ and $\varepsilon_{\infty\parallel}$ are the dielectric constants for light polarized perpendicular and parallel to the tetragonal axis *c*, respectively.

Boltivets *et al.*[6] used optical absorption and photoconductivity measurements to study the fundamental absorption edge of $ZnIn_2Te_4$ and obtained a value of $E_g\sim1.3$ eV at 300 K. Manca *et al.*[7,8] also measured fundamental-reflectivity and photoconductivity spectra of polycrystalline $ZnIn_2Te_4$. They concluded that the material has an indirect gap near 1.40 eV (1.52 eV), as well as the lowest direct gap near 1.87 eV (1.90 eV) at 300 K (85 K). However, this conclusion was obtained relatively easily from the fact that direct transitions generate a peak only in reflectivity, while both direct and indirect transitions are responsible for photoconductivity. Manca *et al.*[7,8] also observed some reflectivity structures at energies ~2.2, 2.4, and 3.6 eV, but gave no detailed discussion of these structures.

In our previous paper[9] we synthesized bulk amorphous $ZnIn_2Te_4$ and measured its pseudodielectric-function spectra by using spectroscopic ellipsometry (SE). The measured spectra showed a strong resemblance to those of amorphous tetrahedrally bonded semiconductors, such as amorphous Si, Ge, and GaAs. The optical energy gap of amorphous $ZnIn_2Te_4$ was determined to be 1.13 eV. Dielectric-related optical constants, such as the complex refractive index, absorption coefficient, and normal-incidence reflectivity, were also presented and modeled using a simplified model of the interband optical transitions.

The purpose of this study is to investigate both experimentally and theoretically the electronic energy-band structure of crystalline $ZnIn_2Te_4$. The experimental techniques used here are optical absorption, SE, and x-ray photoelectron spectroscopy (XPS). The complex dielectric-function spectrum $\varepsilon(E)=\varepsilon_1(E)+i\varepsilon_2(E)$ of a semiconductor is closely related to its electric energy-band structure, which can be drawn from features called critical points (CP's). SE is an excellent technique for investigating the optical response of semiconductors. On-line digitization of the data permits fast and efficient analysis of the structure observed in the spectra in terms of standard analytical line shapes for interband CP's. Numerical differentiation of the data facilitates this analysis. [10] To our knowledge, however, no SE study has been performed on crystalline $ZnIn_2Te_4$ to date. XPS is commonly used for the investigation of the electronic energy-band structure of semiconductors. It is possible to directly determine the core-level energy relative to the valence-band maximum without the need to consider core excitons.[11] The XPS measurements had been performed on almost IV,[12–15] III-V,[13,15,16] and II–VI semiconductors[13,15,16] and also on some ternary chalcopyrite compounds $ZnGeP_2$ and $CdSnAs_2$,[17] but not on $ZnIn_2Te_4$. The band-structure calculation of $ZnIn_2Te_4$ has only been made by Meloni *et al.*[18] They, however, simply assumed $ZnIn_2Te_4$ to have a pseudocubic structure space (group$=V_d^1$), not the actual

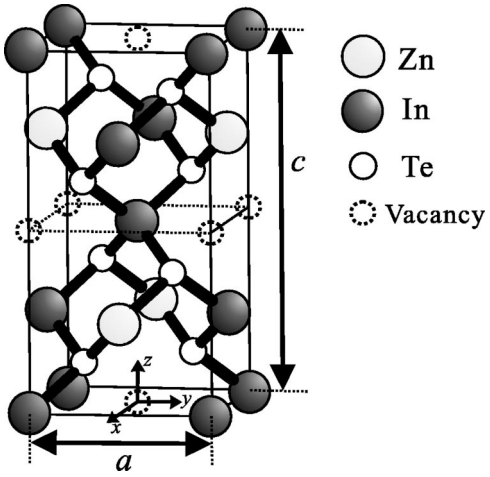

FIG. 1. Crystal structure of defect-chalcopyrite-type semiconductor $ZnIn_2Te_4$.

structure of defect chalcopyrite (S_4^2). The spin-orbit interaction was also neglected in their calculation. We thus calculate the electronic energy-band structure of $ZnIn_2Te_4$, considering the spin-orbit interaction, and compare it with our measured results.

II. EXPERIMENT

The $ZnIn_2Te_4$ crystals used in this study were grown by the conventional Bridgman method. The quartz ampoule graphitized by acetone was filled with a charge of Zn:In:Te $=1:2:4$ mixture in atomic ratio and then sealed off under 10^{-6} Torr. Zn, In, and Te were 99.9999% pure. The ampoule was slowly heated to 1100 °C, melted, and then equilibrated for at least 3 days. The crystals were grown by slowly lowering the ampoule to achieve its cooling rate of ~1.5 °C/h.

The $ZnIn_2Te_4$ crystals obtained were polycrystalline with a grain size of several mm^3. They were not contained spurious phases, such as ZnTe and In_2Te_3. The x-ray diffraction trace for crystalline $ZnIn_2Te_4$ has already been shown in Fig. 1 of Ref. 9. The angles and relative strengths of the diffraction peaks were found to be in good agreement with those reported by Hahn *et al.*[2] ($a=6.11$ Å and $c=12.22$ Å).

The samples used for optical and XPS measurements were prepared by cutting the ingot with a wire saw, by mechanically polishing, and finally by chemically etching with a solution of Br_2 in methanol.

The optical absorption measurements were carried out using a JASCO V-570-DS spectrometer at room temperature. The thickness of the samples used for these measurements was ~0.07 mm.

The SE equipment was of the polarizer–sample–rotating-analyzer type (DVA-36VW-A, Mizojiri Optical, Co, Ltd.). A 150-W xenon lamp was used as the light source. The SE data were measured over the photon-energy range of 1.2–5.5 eV at room temperature. The angle of incidence and the polarizer azimuth were set at 70° and 30°, respectively.

The XPS measurements were performed at room temperature with a ULVAC-PHI model 5600 spectrometer, using Mg$K\alpha_{1,2}$ lines (~1254 eV) as an x-ray source. The taking-off angle of photoelectrons was 45°, and the analyzer pass energy was set at 11.8 eV. Before XPS measurements, argon-ion sputter etching was performed to obtain a clean sample surface.

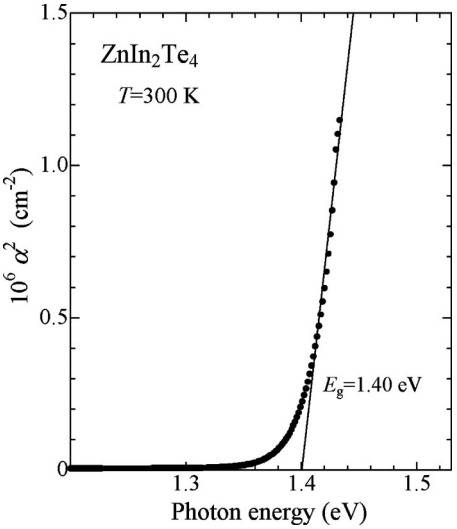

FIG. 2. Square of the absorption coefficient, α^2, as a function of photon energy for $ZnIn_2Te_4$. These plots give an intercept E_0 ~1.40 eV (direct band-gap energy) on the energy axis.

III. RESULTS AND DISCUSSION

A. Optical absorption and SE results

One of the most essential semiconducting parameters is the band-gap energy. In order to obtain the fundamental band-gap energy of $ZnIn_2Te_4$, we have measured the optical absorption spectra of this material. The absorption coefficient α was calculated from the measured transmittance T using the expression

$$T=\frac{(1-R)^2e^{-\alpha x}}{1-R^2e^{-2\alpha x}}, \tag{1}$$

where R is the reflectivity. We used a value of 0.25 for R. This value was obtained from the present study [see Fig. 8(b), below].

Figure 2 plots the square of the absorption coefficient, α^2, as a function of photon energy for $ZnIn_2Te_4$ at room temperature. All the samples measured had appreciable transmission losses (~70 cm^{-1}) in the wavelength region far removed from the absorption edge. We understand that scattering from grain boundaries can account for these losses since they were found to be essentially independent of wavelength. Therefore, these losses were subtracted as the background absorption.

We can see in Fig. 2 that at absorption coefficients above 600 cm^{-1}, the dependence on photon energy E can be written as

$$\alpha(E)=A(E-E_0)^{1/2}. \tag{2}$$

This dependence is expected for direct optical transitions. The plots in Fig. 2 give an intercept E_0~1.40 eV (direct

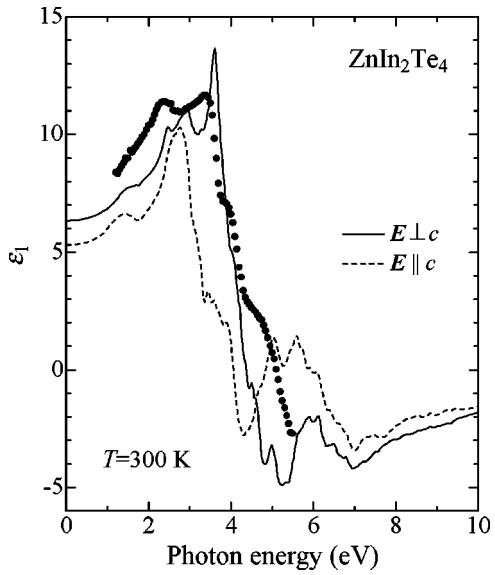

FIG. 3. Pseudodielectric-function spectrum $\varepsilon_1(E)$ for $ZnIn_2Te_4$ measured by SE (solid circles). The solid and dashed lines represent the calculated $\varepsilon_1(E)$ spectra for $\mathbf{E}\perp c$ and $\mathbf{E}\|c$, respectively.

band-gap energy) on the energy axis. We also plotted the dependence upon the photon energy E of $\alpha^{1/2}$. It showed, however, a poorer linear relationship than that in Fig. 2 (α^2). We thus support the contention that $ZnIn_2Te_4$ is a direct band-gap semiconductor. On the contrary, Manca *et al.*[7,8] concluded that it is an indirect band-gap semiconductor. They also concluded that $ZnIn_2Se_4$ (not $ZnIn_2Te_4$) is a direct band-gap semiconductor.

We show in Figs. 3 and 4 the pseudodielectric-function spectra $\varepsilon_1(E)$ (Fig. 3) and $\varepsilon_2(E)$ (Fig. 4) of $ZnIn_2Te_4$ measured by SE (solid circles). The pseudodielectric function is a

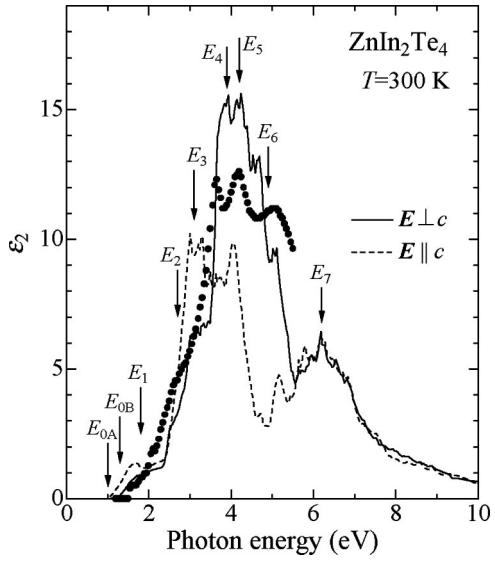

FIG. 4. Pseudodielectric-function spectrum $\varepsilon_2(E)$ for $ZnIn_2Te_4$ measured by SE (solid circles). The solid and dashed lines represent the calculated $\varepsilon_2(E)$ spectra for $\mathbf{E}\perp c$ and $\mathbf{E}\|c$, respectively. The vertical arrows indicate the positions of the CP's (E_0-E_7) found in the calculated $\varepsilon_2(E)$ spectra.

quantity derived from the SE data by means of the two-phase (ambient-substrate) model.[19] It would be exactly equal to the true bulk dielectric function of a given sample if its surface is perfectly abrupt and free from residual overlayers, but these ideal conditions can be never achieved in practice. It is also noted that $ZnIn_2Te_4$ crystallizes in the tetragonal structure. It is thus optically anisotropic and has two dielectric-tensor components $\varepsilon_\perp=\varepsilon_{x,y}$ and $\varepsilon_\|=\varepsilon_z$. While most of the SE works have been confined to optically isotropic materials, the usefulness of this technique in the study of anisotropic systems has been demonstrated.[20] Because of the polycrystalline samples used in this study, we have not tried to measure the optical anisotropy of $ZnIn_2Te_4$ at all.

The experimental $\varepsilon_2(E)$ spectrum shown in Fig. 4 reveals the CP's at ~1.4, 3.6, 4.2, and 5.1 eV. The shoulderlike structures can also be found at ~1.8, 2.1, and 2.6 eV. The ~1.4-eV CP is due to transitions at the fundamental absorption edge (see Fig. 2). The ~2.1, 2.6, and 3.6-eV CP structures agree with those observed in Refs. 7 and 8 (~2.2, 2.4, and 3.6 eV).

The experimental $\varepsilon_2(E)$ spectrum of crystalline $ZnIn_2Te_4$ is quite different from that of amorphous $ZnIn_2Te_4$ (see Fig. 2 in Ref. 9). It is well known that the breakdown of the crystalline periodicity causes the disappearance of the sharp structures found in $\varepsilon(E)$ of the crystalline substance. As seen in Fig. 2, the fundamental absorption gap of crystalline $ZnIn_2Te_4$ is ~1.40 eV. On the other hand, the optical energy gap of amorphous $ZnIn_2Te_4$ was determined to be 1.13 eV.[9] The smaller band gap observed in the amorphous material may be caused by the localized states (i.e., band tail). The maximum in $\varepsilon_2(E)$ of amorphous $ZnIn_2Te_4$ was observed at $E\sim 2.5$ eV, while that in crystalline $ZnIn_2Te_4$ occurs at $E\sim 4$ eV. Such a low-energy shift in the ε_2 maximum has been observed in many amorphous semiconductors.[21]

In order to determine more accurately the CP energy positions, we have performed a second-derivative-fit analysis of the pseudodielectric function using the standard CP model:[10]

$$\frac{d^2\varepsilon(E)}{dE^2}=\begin{cases}-n(n-1)Ae^{i\phi}(E-E_c+i\Gamma)^{n-2}, & n\neq 0,\\ Ae^{i\phi}(E-E_c+i\Gamma)^{-2}, & n=0,\end{cases} \tag{3}$$

where the CP is defined by the amplitude A, CP energy E_c, broadening Γ, and phase angle ϕ. The exponent n has the value $-1/2$ for a one-dimensional CP, 0 [logarithmic, i.e., $\ln(E-E_c+i\Gamma)$] for a two-dimensional CP, and 1/2 for a three-dimensional CP. Discrete excitons can be represented by $n=-1$.

Figure 5 shows the second-derivative spectra $d^2\varepsilon_1(E)/dE^2$ and $d^2\varepsilon_2(E)/dE^2$ for $ZnIn_2Te_4$ (open circles). They are obtained by numerically differentiating the SE$\varepsilon(E)$ data. The solid lines represent fits to Eq. (3). These fits are carried out simultaneously for both the real and imaginary parts using a least-squares fit procedure.

In Fig. 5, the relatively strong structures are identified at 3.60, 4.13, and 5.08 eV. These structures are found to be well fitted with $n=-1$ (i.e., discrete excitons). The weak three-

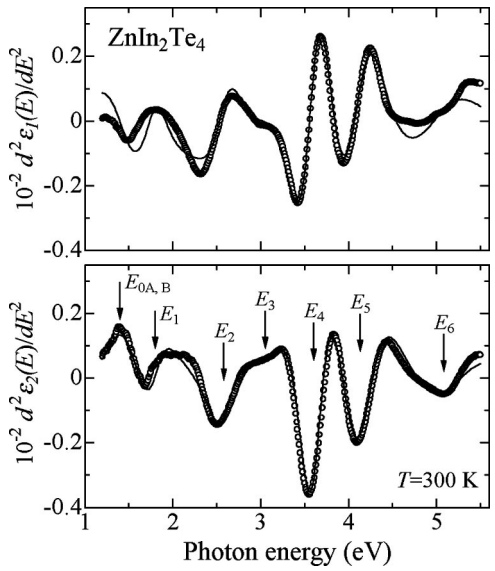

FIG. 5. Second-derivative spectra $d^2\varepsilon_1(E)/dE^2$ and $d^2\varepsilon_2(E)/dE^2$ for $ZnIn_2Te_4$ (open circles). The solid lines represent fits of the second-derivative spectra to Eq. (3). The vertical arrows indicate the positions of the CP's (E_0–E_6) determined from the standard CP fitting. The fit-determined CP parameters are listed in Table I.

dimensional CP's ($n=1/2$) are also identified at energies 1.40, 1.80, 2.58, and 3.05 eV. Table I summarizes these results.

B. Electronic energy-band structure and XPS results

To our knowledge, there has been no study of the band-structure calculation of the defect-chalcopyrite-type semiconductor $ZnIn_2Te_4$. Because of this, we have calculated the electronic energy-band structure of this material based on the empirical pseudopotential method (EPM).[22] The pseudopotential form factors for Zn, In, and Te were extracted from the pseudopotentials of ZnTe and InSb given in Ref. 23. No further attempt was made to fit the pseudopotential to experiment. Because of no experimental information about the spin-orbit splitting of $ZnIn_2Te_4$, we assumed that this material has the same spin-orbit parameter as ZnTe.[24]

Figure 6 shows the calculated energy-band structure of $ZnIn_2Te_4$. The bands are labeled following Refs. 25 and 26. The valence band consists of two subbands separated by ~7 eV [see also Fig. 7(a), below]. The top and bottom valence subbands have widths of about 4 and 1 eV, respectively. The symmetry of the top valence band Γ_{6+7} is p like in nature. The Γ_{5+8} valence bands lie about 0.3 eV below the top valence band Γ_{6+7}, due to the crystal-field splitting. By considering the spin-orbit interaction, the Γ_{2+4} band splits into Γ_{5+8} and Γ_{6+7} bands. The spin-orbit splitting energy is ~0.9 eV. The symmetry of the lowest conduction band Γ_{5+8} is s like in nature. There exist upper conduction bands Γ_{6+7} and Γ_{5+8} at about 1 and 2 eV above the lowest conduction band Γ_{5+8}, respectively. The quadruply degenerated $\Gamma_{5+8}+\Gamma_{6+7}$ conduction bands are also present at ~3.5 eV above the lowest conduction band Γ_{5+8}. The band structure shown in Fig. 6 indicates that $ZnIn_2Te_4$ is a direct band-gap semiconductor, in agreement with our experimental result (Fig. 2).

TABLE I. CP parameters for $ZnIn_2Te_4$ determined by fitting with Eq. (3).

CP	E_c (eV)	n	A (10^4)	ϕ (deg)	Γ (eV)
$E_{0A,B}$	1.40	1/2	15.0	220	0.34
E_1	1.80	1/2	7.0	125	0.22
E_2	2.58	1/2	9.0	80	0.24
E_3	3.05	1/2	4.5	60	0.30
E_4	3.60	−1	1.0	30	0.35
E_5	4.13	−1	1.7	30	0.48
E_6	5.08	−1	2.9	40	0.85

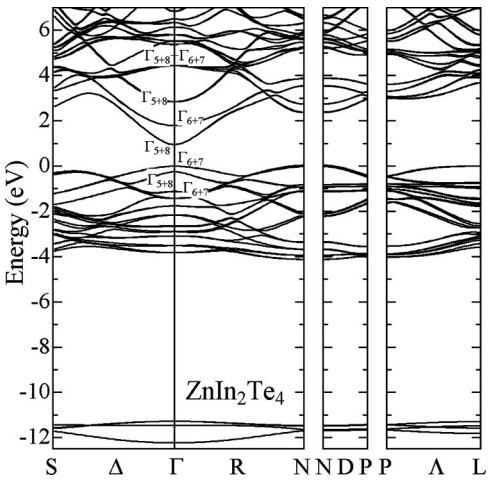

FIG. 6. Electronic energy-band structure of $ZnIn_2Te_4$ calculated by EPM. The numbers denote that of the irreducible representations of double groups.

We have also calculated the density-of-states spectrum $N(E)$ and measured the XPS spectrum $I(E)$. These results are shown in Fig. 7. The $N(E)$ spectrum was plotted by referring to the top of the valence band. The measured $I(E)$ spectrum was corrected for contributions from inelastically scattered electrons.[27]

The strongest peak in $I(E)$ at −10 eV is due to Zn $3d$ core electrons. The two diffuse peaks centered at −1.5 and −4 eV can also be clearly found. These peaks, marked I and II, may correspond to transitions from the upper valence subband having a bandwidth of ~4 eV (see Fig. 6). There is also a shoulder on the low-energy (high-binding-energy) side of the Zn $3d$ peak. This shoulder, marked III, is considered to be due to the lower valence subband centered at −11.5 eV, with a width of ~1 eV [Fig. 7(a)]. The measured $I(E)$ spectrum suggests that the total valence bandwidth in $ZnIn_2Te_4$ is ~14 eV. A broad XPS peak is also found at −7.5 eV. This peak may be due to In $4d$ core electrons excited by Mg $K\alpha_{3,4}$ satellite lines.

The imaginary part of the dielectric function can be calculated from the electronic energy-band structure using the relation[28]

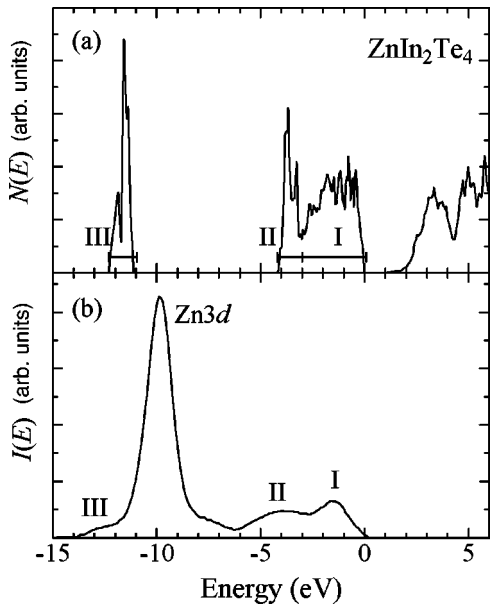

FIG. 7. (a) Theoretical density-of-states spectrum $N(E)$ and (b) experimental XPS spectrum $I(E)$ for $ZnIn_2Te_4$.

$$\varepsilon_2(E)=\frac{e^2\hbar^4}{\theta\pi m^2E^2}\sum_i\sum_{c,\nu}\int\left|\langle\mathbf{k},c|\frac{d}{d\mathbf{x}_i}|\mathbf{k},\nu\rangle\right|^2 \times\delta[E_{c\nu}(\mathbf{k})-E]d\mathbf{k}, \quad (4)$$

where $|\mathbf{k},c\rangle$ and $|\mathbf{k},\mathrm{v}\rangle$ represent the periodic part of the wave functions of the conduction and valence bands, respectively, and $E_{c\nu}(\mathbf{k})$ is the energy difference between the conduction and valence bands. $\theta=2$ and $i=x,y$ correspond to light polarized perpendicular to the c axis ($\mathbf{E}\perp c$), and $\theta=1$ and $i=z$ correspond to light parallel to the c axis ($\mathbf{E}\parallel c$). The integration is performed over the entire Brillouin zone, taking into account $\mathbf{k}$-dependent momentum-matrix element.[29] The real part of the dielectric function $\varepsilon_1(E)$ is obtained by performing a Kramers-Kronig transformation of $\varepsilon_2(E)$.

The solid and dashed lines in Fig. 3 represent the calculated $\varepsilon_1(E)$ spectra of $ZnIn_2Te_4$ for $\mathbf{E}\perp c$ and $\mathbf{E}\parallel c$, respectively. The solid circles show the experimental data. The same results, but for $\varepsilon_2(E)$, are shown in Fig. 4. The CP's obtained from this $\varepsilon_2(E)$ spectrum, with comparison to the experimental data, are given in Table II.

The onset of the absorption edge in the calculated $\varepsilon_2(E)$ spectrum occurs at 1.30 eV for $\mathbf{E}\perp c$ (E_{0B}) and at 0.95 eV for $\mathbf{E}\parallel c$ (E_{0A}). These are the direct band gaps in $ZnIn_2Te_4$ at Γ [$\Gamma_{5+8}\rightarrow\Gamma_{5+8}(\mathbf{E}\perp c)$ and $\Gamma_{6+7}\rightarrow\Gamma_{5+8}(\mathbf{E}\parallel c)$]. The band-structure calculation also suggests the presence of CP's at $\sim$1.8–6.2 eV (E_1–E_7; see Table II). The calculated $\varepsilon_2(E)$ spectrum for $\mathbf{E}\perp c$ is dominated by the E_4 and E_5 peaks, while the prominent peak seen in $\varepsilon_2(E)$ for $\mathbf{E}\parallel c$ is E_3. The E_6 peak is clearly found for $\mathbf{E}\perp c$, but not for $\mathbf{E}\parallel c$.

The contributions to $\varepsilon_2(E)$ of the interband transitions in the specific parts of the Brillouin zone are summarized in Table II. The E_{0A}, E_{0B}, and E_1 structures are dominated by transitions at the Γ point. The E_2 structure may originate from transitions at the N and Γ points for $\mathbf{E}\perp c$ and at the N point for $\mathbf{E}\parallel c$. The E_3 structure may originate mainly from

TABLE II. Experimentally determined CP energies, together with those obtained from the empirical pseudopotential calculation. The valence bands are labeled 1–32 and the conduction bands are from 33. Transitions using these notations are given in parentheses.

		Calc.			
		$\mathbf{E}\perp c$		$\mathbf{E}\parallel c$	
CP	Expt. (eV)	Energy (eV)	Transition	Energy (eV)	Transition
E_{0A}	1.40			0.95	Γ(31,32→33,34)[b]
E_{0B}		1.30	Γ(29,30→33,34)[a]		
E_1	1.80	1.8	Γ(29,30→33,34)[a]	1.8	Γ(31,32→33,34)[b]
E_2	2.58	2.7	N(31,32→33,34)	2.7	N(29,30→33,34)
			Γ(29,30→33,34)[a]		
E_3	3.05	3.1	N(31,32→33,34)	3.1	N(31,32→35,36)
			N(29,30→35,36)		N(29,30→33,34)
E_4	3.60	3.9	N(27,28→35,36)	3.9	N(31,32→39,40)
			P(27,28→35,36)		P(31,32→39,40)
E_5	4.13	4.2	N(25,26→35,36)	4.2	S(27,28→33,34)
			P(25,26→35,36)		S(31,32→37,38)
E_6	5.08	4.9	N(29,30→41,42)		
			P(25,26→39,40)		
			S(27,28→35,36)		
E_7		6.2	N(25,26→43,44)	6.2	N(31,32→53,54)
			L(31,32→49,50)		N(29,30→51,52)
			Γ(31,32→51,52)		

[a] $\Gamma_{5+8}\rightarrow\Gamma_{5+8}$.
[b] $\Gamma_{6+7}\rightarrow\Gamma_{5+8}$.

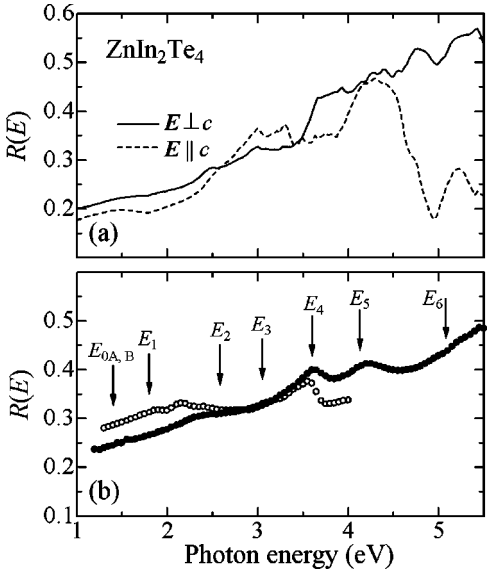

FIG. 8. (a) Theoretical and (b) experimental normal-incidence reflectivity spectra for $ZnIn_2Te_4$. The solid circles are obtained from the SE $\varepsilon(E)$, while the open circles represent the $R(E)$ spectrum measured by Manca *et al.* (Ref. 8). The vertical arrows in (b) indicate the positions of the CP's (E_0-E_6).

transitions at the N point for both $\mathbf{E}\perp c$ and $\mathbf{E}\|c$ polarizations. The E_4 peak is mainly due to transitions at the N and P points for both $\mathbf{E}\perp c$ and $\mathbf{E}\|c$. The E_5 peak is also dominated by transitions at the N and P points for $\mathbf{E}\perp c$ and at the S point for $\mathbf{E}\|c$. The E_6 structure, seen only for $\mathbf{E}\perp c$, arises principally from regions at the N, P, and S points. At higher energy, the E_7 structure may be caused by transitions at the N, L, and Γ points for $\mathbf{E}\perp c$ and at the N point for $\mathbf{E}\|c$.

The optical dielectric constant ε_∞ estimated from the experimental ε_1 spectrum in Fig. 3 is ~ 7.0 $[\varepsilon_\infty=\varepsilon_1(E\rightarrow 0\ \mathrm{eV})]$. This value is in good agreement with that obtained by Neumann *et al.* (7.1 ± 0.3).[5] However, the calculated ε_∞ value (~ 6; see Fig. 3) is slightly smaller than the experimental one. Excitonic effects, electron-phonon interactions, and other many-body corrections may thoroughly influence ε_1 at zero energy. Note that such effects are not included in the present calculation.

Finally, we show in Fig. 8(a) the theoretical normal-incidence reflectivity spectra $R(E)$ for $\mathbf{E}\perp c$ and $\mathbf{E}\|c$ of $ZnIn_2Te_4$. The $R(E)$ spectrum, calculated from the SE $\varepsilon(E)$ data, is plotted in Fig. 8(b) by solid circles. The spectrum measured by Manca *et al.*[8] is also plotted in Fig. 8(b) by open circles. To our knowledge, this was the only optical spectrum measured in the visible-ultraviolet region of $ZnIn_2Te_4$. The experimental R values of ~ 0.4 at the E_4 peak are in reasonable agreement with the theoretical one.

IV. CONCLUSIONS

We have studied the optical properties of the defect-chalcopyrite-type semiconductor $ZnIn_2Te_4$ by means of optical absorption, SE, and XPS. Bulk $ZnIn_2Te_4$ crystals were grown from stoichiometric melts by the conventional Bridgman method. The optical absorption spectrum suggests that the fundamental absorption edge in $ZnIn_2Te_4$ is dominated by direct optical transitions $(E_0\sim 1.40\ \mathrm{eV})$. The complex dielectric-function spectra of $ZnIn_2Te_4$ have been measured by SE in the photon-energy range between 1.2 and 5.5 eV. The measured $\varepsilon(E)$ spectra reveal distinct structures at the E_n CP's $(n=0-6)$. The energy position, strength, and broadening of these CP's have been successfully determined by performing a second-derivative analysis of $\varepsilon(E)$. These CP's have been assigned to specific points in the Brillouin zone by the aid of a band-structure calculation using EPM. The electronic density-of-states spectrum $N(E)$ of $ZnIn_2Te_4$ has also been obtained using XPS and discussed along with the band-structure calculation.

ACKNOWLEDGMENTS

This work is supported in part by a Grant-in-Aid for Encouragement of Young Scientists (S. O.) and a Grant-in Aid for Scientific Research (C) from the Japan Society for the Promotion of Science.

[1] A. N. Georgobiani, S. I. Radautsan, and I. M. Tiginyanu, Sov. Phys. Semicond. **19**, 121 (1985).

[2] H. Hahn, G. Frank, W. Klingler, A. D. Störger, and G. Störger, Z. Anorg. Allg. Chem. **279**, 241 (1955).

[3] O. Madelung, in *Numerical Data and Functional Relationships in Science and Technology*, edited by O. Madelung, Landolt-Börnstein, New Series, Vol. 17h (Springer, Berlin, 1985).

[4] H. Neumann, W. Kissinger, F. Lévy, H. Sobotta, and V. Riede, Cryst. Res. Technol. **25**, 841 (1990).

[5] H. Neumann, W. Kissinger, and F. Lévy, Cryst. Res. Technol. **25**, 1189 (1990).

[6] N. S. Boltivets, V. P. Drobyazko, and V. K. Mityurev, Sov. Phys. Semicond. **2**, 867 (1969).

[7] P. Manca, F. Raga, and A. Spiga, Phys. Status Solidi A **16**, K105 (1973).

[8] P. Manca, F. Raga, and A. Spiga, Nuovo Cimento Soc. Ital. Fis., B **19**, 15 (1974).

[9] Y. Matsumoto, S. Ozaki, and S. Adachi, J. Appl. Phys. **86**, 3705 (1999).

[10] P. Lautenschlager, M. Garriga, and M. Cardona, Phys. Rev. B **36**, 4813 (1987).

[11] M. L. Cohen and J. R. Chelikowsky, *Electronic Structure and Optical Properties of Semiconductors* (Springer, Berlin, 1988), p. 60.

[12] L. Ley, S. Kowalczyk, R. Pollak, and D. A. Shirley, Phys. Rev. Lett. **29**, 1088 (1972).

[13] R. A. Pollak, L. Ley, S. Kowalczyk, D. A. Shirley, J. D. Joannopoulos, D. J. Chadi, and M. L. Cohen, Phys. Rev. Lett. **29**, 1103 (1972).

[14] R. G. Cavell, S. P. Kowalczyk, L. Ley, R. A. Pollak, B. Mills, D.

A. Shirley, and W. Perry, Phys. Rev. B **7**, 5313 (1973).
[15] S. P. Kowalczyk, L. Ley, F. R. McFeely, and D. A. Shirley, J. Chem. Phys. **61**, 2850 (1974).
[16] L. Ley, R. A. Pollak, F. R. McFeely, S. P. Kowalczyk, and D. A. Shirley, Phys. Rev. B **9**, 600 (1974).
[17] C. Varea de Alvarez, M. L. Cohen, L. Ley, S. P. Kowalczyk, F. R. McFeely, D. A. Shirley, and R. W. Grant, Phys. Rev. B **10**, 596 (1974).
[18] F. Meloni, F. Aymerich, G. Mula, and A. Baldereschi, Helv. Phys. Acta **49**, 687 (1976).
[19] R. M. A. Azzam and N. M. Bashara, *Ellipsometry and Polarized Light* (North-Holland, Amsterdam, 1977).
[20] S. Ninomiya and S. Adachi, J. Appl. Phys. **78**, 1183 (1995), and references therein.
[21] J. Tauc, in *Amorphous and Liquid Semiconductors*, edited by J. Tauc (Plenum, London, 1974), p. 195.
[22] C. Varea de Alvarez, M. L. Cohen, S. E. Kohn, Y. Petoroff, and Y. R. Shen, Phys. Rev. B **10**, 5175 (1974).
[23] M. L. Cohen and V. Heine, in *Solid State Physics*, edited by H. Ehrenreich, F. Seitz, and D. Turnbull (Academic, New York, 1970), Vol. 24.
[24] J. P. Walter, M. L. Cohen, Y. Petroff, and M. Balkanski, Phys. Rev. B **1**, 2661 (1970).
[25] D. A. Guseĭnova, T. G. Kerimova, and R. Kh. Nani, Sov. Phys. Semicond. **11**, 670 (1977).
[26] V. L. Panyutin, B. É. Ponedel'nikov, A. É. Rozenson, and V. I. Chizhikov, Izv. Vyssh. Uchebn. Zaved. Fiz. **8**, 57 (1979).
[27] D. E. Eastman, W. D. Grobman, J. L. Freeouf, and M. Erbudak, Phys. Rev. B **9**, 3473 (1974).
[28] M. Y. Au-Yang and M. L. Cohen, Phys. Rev. **178**, 1279 (1969).
[29] G. Gilat and N. R. Bharatiya, Phys. Rev. B **12**, 3479 (1975).